JCTC Journal of Chemical Theory and Computation

Article

pubs.acs.org/JCTC

Analytic Molecular Hessian Calculations for CC2 and MP2 Combined with the Resolution of Identity Approximation

Daniel H. Friese,*[,†] Christof Hättig,*[,†] and Jörg Koβmann*[,‡]

[†]Lehrstuhl für Theoretische Chemie, Ruhr-Universität Bochum, D-44801 Bochum, Germany

[‡]Atomistic Modelling and Simulation, ICAMS, Ruhr-Universität Bochum, D-44801 Bochum, Germany

Supporting Information

ABSTRACT: An implementation of analytic second derivatives for the approximate coupled cluster singles and doubles model CC2 and for second-order Møller−Plesset perturbation theory (MP2) will be presented. The RI approximation for the two-electron repulsion integrals is used to reduce memory demands, operation count, and I/O requirements. During the calculation, the storage of $\mathcal{N}^4$ quantities (where $\mathcal{N}$ is a measure for the system size) can completely be avoided. It is shown that with the MP2 method and an appropriate scaling of the harmonic frequencies, especially C−F stretch frequencies are reproduced much better in comparison to experiments than with the B3LYP density functional. Similar advantages are observed for molecules with strong, internal van der Waals interactions. Spin scaling offers additional improvements in these cases. The implementation has been tested for molecules with up to 81 atoms and 684 basis functions.

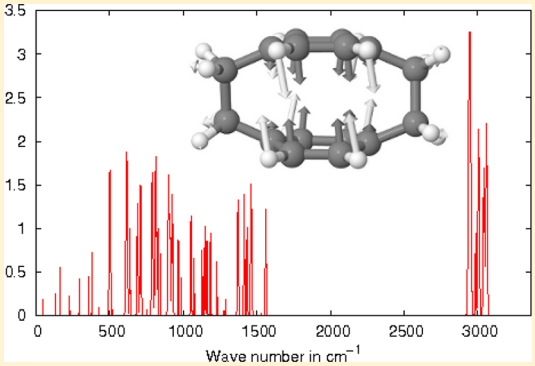

1. INTRODUCTION

Due to the important role vibrational spectroscopy plays in many parts of chemistry, the calculation of vibrational spectra has been an important task of quantum chemical calculations for several decades. Accurate calculations for vibrational frequencies of polyatomic molecules are even in the harmonic approximation still a challenge for quantum chemistry due to the high computational cost and the complexity of the corresponding implementations, which exceeds by far the effort which is needed for energy and gradient calculations. The Hessian requires the computation of the first-order wave function, which is not needed for the gradient. This is also the reason why calculation times for the Hessian show a steeper scaling with the system size than gradient calculations.

Lots of implementations for a large variety of methods have been presented, especially in the field of density functional theory (DFT).[1] Works of Radom et al. have shown that DFT, especially with the well-established B3LYP functional,[2−6] is a very reliable and efficient tool to calculate vibrational spectra, especially when they are combined with scaling factors as a correction for the errors due to the anharmonicity and the chosen method.[7,8] Concerning infrared intensities, similar findings have been made by Halls and Schlegel.[9] Therefore, it can be assumed that DFT is the method of choice for vibrational spectra calculations of polyatomic molecules.

Nevertheless, the limited applicability of DFT methods for weakly bound systems[10] has induced the development of several DFT methods which make use of orbital-dependent correlation, which can be introduced, e.g., via MP2-like contributions.[11,12] For the enhancement of this type of density functionals to the calculation of vibrational spectra, an efficient implementation of the molecular Hessian with correlated wave function based methods and especially Møller−Plesset perturbation theory of second order (MP2) is an essential requirement. Since MP2 is the simplest correlated wave function based method, a Hessian implementation for MP2 is also an important keystone for the implementation of Hessians with other correlated wave function based methods, namely with coupled cluster techniques which are capable of treating excited states.

The oldest successful method to calculate molecular Hessians is a half-numerical ansatz which has been introduced by Pulay et al. in 1969 where analytical gradients are differentiated numerically.[13] Nevertheless, even before that Bishop and Randič pointed out that a fully analytic treatment would result in a higher accuracy.[14] The latter is important for the computation of third and fourth derivatives of the energy by numerical differentiation of the Hessian, e.g., for quartic force fields. With the usual double precision floating point arithmetic, a 3-fold numerical differentiation of analytic gradients is for most purposes not accurate enough.

Gauss and Stanton give an overview of the challenges which have restrained the development of fully analytic molecular Hessian implementations for correlated wave function based methods for a long time.[15] Analytic second-order derivatives for the MP2 method were reported first in 1985 and 1986.[16,17] The use of such methods for second-order derivative calculations is

Received: January 15, 2013
Published: February 28, 2013

still restricted to very small molecules due to its steep $\mathcal{N}^6$-scaling behavior where $\mathcal{N}$ is a measure for the system size. A treatment in the framework of response theory was presented by Helgaker and co-workers.[18,19] In the field of coupled cluster theory, an implementation of molecular Hessians for the coupled cluster singles and doubles model (CCSD) has been reported by Koch et al.[20] and Kállay and Gauss have presented a general implementation that is compatible with a variety of coupled cluster models.[21] Gauss and Stanton have reported a Hessian implementation for the CCSD(T) and CCSDT models.[22,23]

The approximate coupled cluster singles and doubles model CC2 was first introduced by Christiansen et al.[24] as an approximation to CCSD which can be applied in the framework of coupled cluster response theory and is therefore capable of treating excited states. CC2 expressions for most properties can easily be simplified to MP2 expressions, which means that implementations of Hessians and dipole gradients for CC2 and MP2 can be combined. A CC2 implementation for molecular Hessians is of special interest since it can be extended to the treatment of excited states.

The introduction of inner projection techniques such as Cholesky decomposition[25] or the RI approximation (also known as "density fitting")[26−29] into the MP2 model and the closely related CC2 method has made these approaches applicable to molecules with more than a dozen atoms for calculations of excitation energies,[30] first-order molecular properties,[31] energy gradients for ground and excited states,[32−34] second-order one-electron properties,[35,36] and two-photon absorption matrix elements.[37]

In the following, we will present an analytic implementation of molecular Hessians and dipole moment derivatives for the MP2 and CC2 methods which use the resolution of identity (RI) approximation to reduce both operation count and the demand of memory and disc space. Special effort is made to avoid storage of $\mathcal{N}^4$-scaling quantities.

The remainder of this paper is organized at follows: In section 2 we will present our working equations, while in section 3 we will focus on the key features of our implementation and examine the error due to the newly introduced approximation. In section 4 we will present some applications, and in section 5 we will give some concluding remarks.

2. THEORY

In the following, we present the working equations for the CC2 method in the closed-shell case. The corresponding equations for MP2 are obtained by neglecting all terms that contain singles cluster amplitudes or Lagrangian multipliers.

2.1. The CC2 Lagrangian and the RI-CC2 Approach.

Second derivatives of the energy are for nonvariational methods conveniently obtained using the Lagrangian technique.[20,33,38,39] The Lagrangian for CC2 including orbital relaxation is:[24,39]

$$\begin{aligned} L^{\mathrm{CC2}} = {} & \langle \mathrm{HF}|\hat{\hat{H}} + [\hat{\hat{H}}, \hat{T}_2]|\mathrm{HF}\rangle + \sum_{\mu_1} \overline{t}_{\mu_1}\langle \mu_1|\hat{\hat{H}} \\ & + [\hat{\hat{H}}, \hat{T}_2]|\mathrm{HF}\rangle + \sum_{\mu_2} \overline{t}_{\mu_2}\langle \mu_2|\hat{\hat{H}} + [\hat{\hat{F}}, \hat{T}_2]|\mathrm{HF}\rangle \\ & + \sum_{\mu_0} \overline{\kappa}_{\mu_0} F_{\mu_0} \end{aligned} \tag{1}$$

where $\hat{T}_i$ denotes the cluster operator for the excitation level i defined as

$$\hat{T}_i = \sum_{\mu_i} t_{\mu_i}\tau_{\mu_i} \tag{2}$$

In the last equation, t_{μ_i} represents the cluster amplitudes and τ_{μ_i} the excitation operators generating the excitations μ_i. $\hat{\hat{O}}$ denotes $\hat{T}_1$ similarity transformed operators defined as

$$\hat{\hat{O}} = \mathrm{e}^{-\hat{T}_1}\,\hat{O}\,\mathrm{e}^{\hat{T}_1} \tag{3}$$

$\overline{t}_{\mu_1}$ and $\overline{t}_{\mu_2}$ are the Lagrangian multipliers for the singles (μ_1) and doubles (μ_2) excitation manifolds. F is the Fock matrix, and $\hat{F}$ is the corresponding Fock operator. The last term in eq 1 accounts for the equations which determine the orbital rotation parameters κ_{μ_0} by requiring that the Fock matrix elements F_{μ_0} vanish and $\overline{\kappa}_{\mu_0}$ are the corresponding Lagrangian multipliers.

In the following, the Hamiltonian $\hat{\hat{H}}$ for a closed-shell system will be treated in terms of second quantization. According to Helgaker et al., it is given by[40]

$$\hat{\hat{H}} = \sum_{pq} \hat{h}_{pq}E_{pq} + \frac{1}{2}\sum_{pqrs} (pq\hat{|}rs)\, e_{pqrs} \tag{4}$$

where p, q, r, and s denote both occupied and virtual molecular orbitals. E_{pq} and e_{pqrs} are the usual spin-free one- and two-particle operators and $\hat{h}_{pq}$ and $(pq\hat{|}rs)$ denote the one- and two-electron integrals in the $\hat{T}_1$ similarity transformed molecular orbital (MO) basis.

The two terms linear in the Lagrangian multipliers $\overline{t}_{\mu_1}$ and $\overline{t}_{\mu_2}$ in eq 1 are the CC2 ground state equations. From the CC2 doubles equation, the doubles cluster amplitudes can be written assuming canonical MOs as

$$t_{ij}^{ab} = -\frac{(ai\hat{|}bj)}{\varepsilon_a - \varepsilon_i + \varepsilon_b - \varepsilon_j} \tag{5}$$

where ε_p is the energy of orbital p. Here and in the following, we use the convention that indices i, j, k... refer to occupied and a, b, c... to virtual molecular orbitals. The Lagrangian for the MP2 energy is obtained as a simplification of eq 1 by omitting the contributions from singles cluster amplitudes and Lagrangian multipliers.

Following refs 33 and 34, the Lagrangian can be expressed using the one-electron densities D^{F} and D^{SCF} (which correspond to the unrelaxed contributions to relaxed CC2 (or MP2) and the SCF one-electron densities and form the so-called "separable part" of the two-electron density) and the nonseparable part of the two-electron density $\hat{d}^{\mathrm{nsep}}_{pqrs}$ for a closed-shell Hartree−Fock reference determinant as

$$\begin{aligned} L^{\mathrm{CC2}} = {} & \sum_{pq} (D^{\mathrm{F}}_{pq} + D^{\mathrm{SCF}}_{pq} + \overline{\kappa}_{pq})F_{pq} \\ & - \frac{1}{8}\sum_{pqrs} D^{\mathrm{SCF}}_{pq}D^{\mathrm{SCF}}_{rs}A^{\mathrm{CPHF}}_{pqrs} + \frac{1}{2}\sum_{pqrs} \hat{d}^{\mathrm{nsep}}_{pqrs}(pq\hat{|}rs)^{\mathrm{RI}} \end{aligned} \tag{6}$$

$$A^{\mathrm{CPHF}}_{pqrs} = 4(pq|rs) - (ps|rq) - (pr|sq) \tag{7}$$

where $(pq\hat{|}rs)^{\mathrm{RI}}$ denotes two-electron integrals in the RI approximation (*vide infra*). The first term is referred to as

the "one-electron part," while the two other terms are called "two-electron parts."

In RI-CC2 and RI-MP2, the two-electron integrals in eq 5 and the last term of eq 6 are expanded in an auxiliary basis[30] and expressed in terms of three-index intermediates as

$$(pq\hat{|}rs) \approx \sum_{Q} \hat{B}^{Q}_{pq}\hat{B}^{Q}_{rs} \tag{8}$$

where Q is an auxiliary basis function and

$$\hat{B}^{Q}_{pq} = \sum_{P} (pq\hat{|}P)[\mathbf{V}^{-1/2}]_{PQ} \tag{9}$$

$V_{PQ} = (P|Q)$ and $(pq|\hat{P})$ are, respectively, two- and three-index electron repulsion integrals (ERIs), where for the latter the indices p and q are in the similarity-transformed MO basis. The RI approximation for the integrals will in the following be used for the nonseparable part of eq 6 while the separable part is computed with usual four-index integrals. Thus, only the Hartree−Fock contributions to the energy and the Fock matrix are evaluated with the exact four-index ERIs. In particular, the CC2 doubles cluster amplitudes (eq 5) can be rewritten using the B^{Q} intermediates according to ref 30.

With this approach and the occasional use of a numerical Laplace transformation[36,41,42] (*vide infra*), the storage of four-index integrals, doubles amplitudes, and other quantities of comparable size can completely be avoided since it becomes feasible to calculate them from three-index intermediates on-the-fly whenever needed and contract them immediately to lower dimensional arrays, which can easily be stored in memory or on disc.

2.2. Derivatives of the Lagrangian. The second derivative of eq 1 with respect to two geometrical distortions x and y is expressed using the well established $2n + 1$ and $2n + 2$ rules[39] for the cluster amplitudes, the orbital rotation parameters, and the corresponding Lagrangian multipliers as[20,38]

$$\left(\frac{d^2L^{\mathrm{CC2}}}{dxdy}\right)_{x,y=0} = \langle \hat{J}^{xy}\rangle + \mathbf{F}\cdot t^x\cdot t^y + \eta^x\cdot t^y + \eta^y\cdot t^x \tag{10}$$

with

$$F_{\mu\nu} = \left(\frac{\partial^2 L^{\mathrm{CC2}}}{\partial t_\mu \partial t_\nu}\right)_{x,y=0} \tag{11}$$

$$\eta^x_\mu = \left(\frac{\partial^2 L^{\mathrm{CC2}}}{\partial t_\mu \partial x}\right)_{x=0} + \sum_\nu \left(\frac{\partial^2 L^{\mathrm{CC2}}}{\partial t_\mu \partial \kappa_\nu}\right)_{x=0} \kappa^x_\nu \tag{12}$$

$$\begin{aligned}\hat{J}^{xy} = {} & \hat{H}^{[xy]} + \hat{P}^{xy}\left(\kappa^x - \frac{1}{2}S^{[x]}, \hat{H}^{[y]}\right) \\ & + \frac{1}{4}\hat{P}^{xy}(S^{[x]}S^{[y]} - S^{[xy]}, \hat{H}) + \frac{1}{4}(S^{[x]}, S^{[y]}, \hat{H}) \\ & + (\kappa^x, \kappa^y, \hat{H}) - \frac{1}{2}\hat{P}^{xy}(\kappa^x, (S^{[y]}, \hat{H}))\end{aligned} \tag{13}$$

Above, $\hat{P}^{xy}$ is a permutation operator defined by $\hat{P}^{xy}f(x,y) = f(x,y) + f(y,x)$, and t^x denotes the first derivatives of the cluster amplitudes with respect to a perturbation x while κ^x are the first derivatives of the orbital rotation parameters. $S^{[x]}$ and $S^{[xy]}$ are the first and second derivatives of the overlap matrix in the basis of the unmodified molecular orbitals (UMO).[43] The terms in parentheses in eq 13 denote one-index transformations of the Hamiltonian with the corresponding matrices following the lines of ref 43. While the index x indicates a complete derivative, the indices $[x]$ and $[xy]$ denote first and second derivatives in the atomic orbitals only. $\hat{H}^{[x]}$ and $\hat{H}^{[xy]}$ therewith are Hamiltonians in second quantization which are constructed from derivatives of the AO integrals transformed to the UMO basis.

The contraction with the cluster amplitude Hessian $\mathbf{F}$ vanishes for MP2. Explicit working expressions for the implementation of the contraction $\mathbf{F}\cdot t^x\cdot t^y$ for RI-CC2 have been reported in ref 36 in the context of frequency-dependent polarizabilities. They will not further be discussed here since they are not influenced by the additional intermediates resulting from geometrical derivatives. The term η^x is expressed in a density-based form (*vide infra*) as is the CC2 or MP2 expectation value $\langle \hat{J}^{xy}\rangle$ of the effective second-order Hamiltonian $\hat{J}^{xy}$, which has been defined in eq 13.

The parameters κ^x are obtained from the solution of the coupled-perturbed Hartree−Fock (CPHF) equations

$$\kappa^x_{ai}(\varepsilon_i - \varepsilon_a) - \sum_{bj} A^{\mathrm{CPHF}}_{aibj}\kappa^x_{bj} = \xi^{[x],\mathrm{CPHF}}_{ai} \tag{14}$$

where $\mathbf{A}^{\mathrm{CPHF}}$ is the CPHF matrix defined in eq 7 and $\xi^{[x],\mathrm{CPHF}}$ is the corresponding right-hand side vector,[18,19] which is defined in the Supporting Information.

2.3. The Expectation Value of $\langle \hat{J}^{xy}\rangle$. To evaluate $\langle \hat{J}^{xy}\rangle$, we first combine κ^x and $\mathbf{S}^{[x]}$ as

$$\mathbf{U}^x = \kappa^x - \frac{1}{2}\mathbf{S}^{[x]} \tag{15}$$

so that the complete first derivative of the MO coefficient matrix is obtained as $\mathbf{C}^x = \mathbf{C}\cdot\mathbf{U}^x$, where $\mathbf{C}$ is the (undifferentiated) MO coefficient matrix. Plugging eq 15 into eq 13 and forming the expectation value, we obtain

$$\begin{aligned}\langle \hat{J}^{[xy]}\rangle = {} & \langle \hat{H}^{[xy]}\rangle + \hat{P}^{xy}\langle (U^y, \hat{H}^{[x]})\rangle - \frac{1}{2}\langle (S^{[xy]}, \hat{H})\rangle \\ & + \langle (U^x, U^y, \hat{H})\rangle - \frac{1}{2}\hat{P}^{xy}\langle ((U^y, S^{[x]}), \hat{H})\rangle\end{aligned} \tag{16}$$

The first term of eq 16 accounts for the second derivatives of the AO integrals in the Hamiltonian $\hat{H}$ and is expressed—using eq 6—as

$$\begin{aligned}\langle \hat{H}^{[xy]}\rangle = {} & \sum_{pq}(D^{\mathrm{F}}_{pq} + D^{\mathrm{SCF}}_{pq} + \bar{\kappa}_{pq})F^{[xy]}_{pq} \\ & - \frac{1}{8}\sum_{pqrs} D^{\mathrm{SCF}}_{pq}D^{\mathrm{SCF}}_{rs}A^{\mathrm{CPHF},[xy]}_{pqrs} + \frac{1}{2}\sum_{pqrs}\hat{d}^{\mathrm{nsep}}_{pqrs}\hat{P}^{pq}_{rs} \\ & \sum_{Q}(\hat{B}^{Q,[xy]}_{pq}\hat{B}^{Q}_{rs} + \hat{B}^{Q,\{x\}}_{pq}\hat{B}^{Q,\{y\}}_{rs})\end{aligned} \tag{17}$$

In the last equation, we introduced the permutation operator $\hat{P}^{pq}_{rs}f_{pq,rs} = f_{pq,rs} + f_{rs,pq}$. $F^{[xy]}$ is the Fock matrix constructed from second derivatives of the one- and two-electron integrals and $A^{\mathrm{CPHF},[xy]}_{pqrs}$, the second derivative of the CPHF matrix. $\hat{B}^{Q,\{x\}}_{pq}$ and $\hat{B}^{Q,[xy]}_{pq}$ are intermediates involving the first and second derivatives of the two-electron integrals in the UMO basis. The detailed expressions for them are

dx.doi.org/10.1021/ct400034t | J. Chem. Theory Comput. 2013, 9, 1469−1480

$$\hat{B}^{Q,\{x\}}_{pq} = \sum_{\alpha\beta} \Lambda^{p}_{\alpha p}\Lambda^{h}_{\beta q}\left(\sum_{P} (\alpha\beta|P)^{[x]}[\mathbf{V}^{-1/2}]_{PQ} - \sum_{P} (\alpha\beta|P) \sum_{RS} [\mathbf{V}^{-1}]_{PR} V^{[x]}_{RS}[\mathbf{V}^{-1/2}]_{SQ}\right) \tag{18}$$

$$\hat{B}^{Q,[xy]}_{pq} = \sum_{\alpha\beta} \Lambda^{p}_{\alpha p}\Lambda^{h}_{\beta q}\left(\sum_{P} (\alpha\beta|P)^{[xy]}[\mathbf{V}^{-1/2}]_{PQ} - \frac{1}{2}\sum_{P} (\alpha\beta|P) \sum_{RS} [\mathbf{V}^{-1}]_{PR} V^{[xy]}_{RS}[\mathbf{V}^{-1/2}]_{SQ}\right) \tag{19}$$

Here, Λ^p and Λ^h denote transformation matrices from the AO basis to the $\hat{T}_1$ similarity transformed MO basis as defined in the Supporting Information.

Equation 17 is further simplified to avoid storage of $\mathcal{N}^4$ quantities: The contractions of second derivatives of the two-electron integrals with the one- and two-particle densities are evaluated using integral-direct algorithms in the AO basis. The separable part is treated using exact four-index integrals, while the nonseparable part is evaluated via two- and three-index two-electron integrals and densities. Exploiting the particle exchange symmetry between the index pairs $\alpha\beta$ and $\gamma\delta$, we can write eq 17 in the AO basis as

$$\langle \hat{H}^{[xy]} \rangle = \sum_{pq} D^{\mathrm{eff}}_{\alpha\beta} h^{[xy]}_{\alpha\beta} + \frac{1}{4}\sum_{\alpha\beta}\left(D^{\mathrm{eff}}_{\alpha\beta} - \frac{1}{2}D^{\mathrm{SCF}}_{\alpha\beta}\right) \sum_{\gamma\delta} A^{\mathrm{CPHF},[xy]}_{\alpha\beta\gamma\delta} D^{\mathrm{SCF}}_{\gamma\delta} + \sum_{\alpha\beta Q} \Delta^{Q}_{\alpha\beta}(\alpha\beta|Q)^{[xy]} - \sum_{PQ} \gamma_{PQ} V^{[xy]}_{PQ} + \frac{1}{2}\hat{P}^{xy}\left(\sum_{\alpha\beta Q} \Delta^{Q,[x]}_{\alpha\beta}(\alpha\beta|Q)^{[y]} - \sum_{PQ} \gamma^{[x]}_{PQ} V^{[y]}_{PQ}\right) \tag{20}$$

where γ_{PQ} and $\Delta^{Q}_{\alpha\beta}$ denote two- and three-index two-electron densities defined in the Supporting Information.

The unperturbed densities D^{eff}_{pq}, $\Delta^{Q}_{\alpha\beta}$, and γ_{PQ} are the same as used in the evaulation of the ground state gradient as described in ref 33 where also detailed working expressions are given. They are contracted with the second derivatives of the AO integrals using the same integral-direct algorithm as described for the gradient with the first derivatives of the integrals.

The second term of eq 16 corresponds to a one-index transformation of the first-order Hamiltonian $\hat{H}^{[x]}$ with the matrix U^y.[44] The double one-index transformation in the fourth term in eq 16 can be rewritten such that it consists of two nested one-index transformations according to

$$\langle (U^y, U^x, \hat{H})\rangle = \frac{1}{2}\langle (U^y, (U^x, \hat{H}))\rangle + \frac{1}{2}\langle (U^x, (U^y, \hat{H}))\rangle \tag{21}$$

Using eq 21, the contributions of the second and the fourth term can be composed to one contribution by introducing the operator $\hat{\mathcal{J}}^x$:

$$\hat{\mathcal{J}}^x = \hat{H}^{[x]} + \frac{1}{2}(U^x, \hat{H}) \tag{22}$$

Therefore, the second and fourth terms of eq 16 are written as expectation values of the one-index transformed operator as

$$\langle (U^y, \hat{\mathcal{J}}^x)\rangle = \sum_{pq} (D^{F}_{pq} + D^{\mathrm{SCF}}_{pq} + \bar{\kappa}_{pq})(U^y, F[\hat{\mathcal{J}}^x])_{pq} - \frac{1}{8}\sum_{pqrs} D^{\mathrm{SCF}}_{pq} D^{\mathrm{SCF}}_{rs}(U^y, A^{\mathrm{CPHF}}[\hat{\mathcal{J}}^x])_{pqrs} + \sum_{pqrs} \hat{d}^{nsep}_{pqrs}(U^y, \sum_{Q} \hat{B}^{Q}\hat{B}^{Q}[\hat{\mathcal{J}}^x])_{pqrs} \tag{23}$$

This expression is simplified by extracting the transformation with U^y from the integral-density contractions and forming perturbed effective Fock matrices (which correspond to the unperturbed effective Fock matrix in ref 33) which are then contracted with the matrix U^y to form the expectation value according to

$$\langle (U^y, \hat{\mathcal{J}}^x)\rangle = \sum_{pq} U^{y}_{pq} F^{\mathrm{eff},x}_{pq} \tag{24}$$

Explicit expressions for the effective Fock matrix $F^{\mathrm{eff},x}$ are given in the Supporting Information.

The third and fifth term in eq 16 correspond to the expectation value of a zeroth-order Hamiltonian, which is one-index transformed with the second dervative of the overlap matrix $S^{xy} = S^{[xy]} + \hat{P}^{xy}(U^y, S^{[x]})$. Similar to eq 24, these contributions are rewritten as a contraction with the unperturbed effective Fock matrix F^{eff}:

$$\frac{1}{2}\langle (S^{xy}, \hat{H})\rangle = \frac{1}{2}\sum_{pq} S^{xy}_{pq} F^{\mathrm{eff}}_{pq} \tag{25}$$

2.4. The Response of the Cluster Amplitudes.

Following the lines of response theory, the first derivative of the cluster amplitudes is obtained from a linear equation system[45]

$$\mathbf{A}\mathbf{t}^x = \xi^x \tag{26}$$

where $\mathbf{A}$ is the coupled cluster Jacobi matrix:

$$\mathbf{A}_{\mu\nu} = \left(\frac{\partial^2 L}{\partial \bar{t}_\mu \partial t_\nu}\right)_{\varepsilon=0} \tag{27}$$

Working equations for the CC2 Jacobi matrix have already been reported in refs 24 and 30. The explicit expressions for the singles and doubles parts of ξ^x are[36]

$$\xi^{x}_{ai} = \sum_{ck} (2t^{ac}_{ik} - t^{ac}_{ki})F_{kc}[\hat{J}^x] + \hat{F}_{ai}[\hat{J}^x] + \sum_{cdk} (2t^{cd}_{ik} - t^{cd}_{ki})\hat{P}^{ka}_{dc}\sum_{Q} B^{Q}_{kd}[\hat{J}^x]\hat{B}^{Q}_{ac} + \sum_{dkl} (2t^{ad}_{kl} - t^{ad}_{lk})\hat{P}^{lk}_{di}\sum_{Q} B^{Q}_{ld}[\hat{J}^x]\hat{B}^{Q}_{ki} \tag{28}$$

dx.doi.org/10.1021/ct400034t | J. Chem. Theory Comput. 2013, 9, 1469−1480

$$\xi^x_{aibj} = \hat{P}^{ab}_{ij}\left(\sum_c t^{ac}_{ij}F_{cb}[\hat{f}^x] - \sum_k t^{ab}_{ik}F_{kj}[\hat{f}^x] + \sum_Q \hat{B}^Q_{ai}[\hat{f}^x]\hat{B}^Q_{bj}\right) \tag{29}$$

Here $F[\hat{f}^x]_{pq}$ is the perturbed Fock matrix[20] and $B[\hat{f}^x]_{pq}$ the corresponding three-index intermediates:

$$B^Q_{pq}[\hat{f}^x] = \sum_P \left\{(\alpha\beta|P)^{[x]} - \frac{1}{2}\sum_S (\alpha\beta|S) \sum_R [V^{-1}]_{SR}V^{[x]}_{RP}\right\}[V^{-1/2}]_{PQ} \tag{30}$$

$\hat{F}[\hat{f}^x]_{pq}$ and $\hat{B}[\hat{f}^x_{pq}]$ are formed from perturbed one-index transformed integrals. In contrast to the expressions discussed in ref 36, $\hat{F}[\hat{f}^x]_{pq}$ contains through U^x the derivatives of the overlap matrix and contributions from the derivatives of AO two-, three-, and four-index two-electron integrals.

Since the doubles−doubles block of the Jacobi matrix for CC2 is diagonal in the canonical MO basis, an iterative solution of a linear equation system (LES) according to eq 26 can be avoided for the response of the doubles amplitudes if the LES is reduced to an effective LES within the singles space only, according to refs 30 and 31. This enables us to avoid storage of ξ^x_{aibj} as well as storage of the corresponding trial and solution vectors. Explicit expressions for the CC2 effective Jacobi matrix were reported in ref 24. After the solution of the linear response equations for the first-order singles amplitudes, the doubles amplitudes can be obtained from a noniterative expression according to

$$t^{ab,x}_{ij} = -\frac{\xi^x_{aibj} + \sum_Q \hat{P}^{ab}_{ij}\bar{B}^{Q,x}_{ai}\hat{B}^Q_{bj}}{\varepsilon_a - \varepsilon_i + \varepsilon_b - \varepsilon_j} \tag{31}$$

with the three-index intermediates $\bar{B}^{Q,x}_{ai}$ defined as

$$\bar{B}^{Q,x}_{ai} = \sum_{\alpha\beta}(\bar{\Lambda}^{p,x}_{\alpha a}\Lambda^h_{\beta i} + \Lambda^p_{\alpha a}\bar{\Lambda}^{h,x}_{\beta i})\sum_P (\alpha\beta|P)[V_{PQ}]^{-1/2} \tag{32}$$

Explicit definitions of the matrices $\bar{\Lambda}^{p,x}$ and $\bar{\Lambda}^{h,x}$ are given in the Supporting Information. For MP2, eq 31 simplifies to

$$t^{ab,x}_{ij} = -\frac{P^{ab}_{ij}(\sum_c t^{ac}_{ij}F_{cb}[\hat{f}^x] - \sum_k t^{ab}_{ik}F_{kj}[\hat{f}^x] + \sum_Q B^Q_{ai}[\hat{f}^x]B^Q_{bj})}{\varepsilon_a - \varepsilon_i + \varepsilon_b - \varepsilon_j} \tag{33}$$

2.5. The Contraction of the Two-Electron Density d^η with Integrals. To avoid storage of the two-particle part of the vector η, the dot product $\eta^x\cdot t^y$ (see eqs 10 and 12) is rewritten to contractions of perturbed Fock matrices and two-electron integrals in the RI approximation with two- and three-index densities:

$$\eta^x\cdot t^y = \sum_{pq} D^{F,\eta,y}_{pq}F_{pq}[\hat{f}^x] + \sum_{pqQ}\left(\sum_{rs}\hat{B}^Q_{rs}\hat{d}^{nsep,\eta,y}_{pqrs}\right)\hat{B}^Q_{pq}[\hat{f}^x] \tag{34}$$

The densities $D^{F,\eta,y}$ and $\hat{d}^{nsep,\eta,y}$ compile cluster amplitudes and Lagrangian multipliers and depend on only one of the two perturbations. Explicit expressions for the densities are given in the Supporting Information.

To avoid a simultaneous storage of $\bar{B}^Q_{pq}[\hat{f}^x]$ for many perturbations, eq 34 is separated into four parts connected with the derivatives of the three- and two-index two-electron integrals and the derivatives of the MO coefficients:

$$\eta^x\cdot t^y = \sum_{pq} D^{F,\eta,y}_{pq}F_{pq}[\hat{f}^x] + \sum_{\alpha\beta Q}\Delta^{Q,\eta,y}_{\alpha\beta}(\alpha\beta|Q)^{[x]} + \sum_{PQ}\gamma^{\eta,y}_{PQ}V^{[x]}_{PQ} + \sum_{pq}F^{eff,\eta,y}_{pq}U^x_{pq} \tag{35}$$

In the last equation, $\Delta^{Q,\eta,y}_{\alpha\beta}$ and $\gamma^{\eta,y}_{PQ}$ denote three- and two-index two-electron densities, respectively, and $F^{eff,\eta,y}_{pq}$, the effective Fock matrices. Explicit expressions for $F^{eff,\eta,y}_{pq}$ are given in the Supporting Information. Here, we only note that similar to the unperturbed densities also $\Delta^{Q,\eta,y}_{\alpha\beta}$ is obtained by contracting the four-index two-particle density $\hat{d}^{nsep,\eta,y}_{pqrs}$ with three-index electron repulsion integrals according to

$$\Delta^{Q,\eta,y}_{\alpha\beta} = \sum_{\alpha\beta}\Lambda^p_{\alpha p}\Lambda^h_{\beta q}\sum_{rsP}\hat{d}^{\eta,nsep,y}_{pqrs}(rs|P)[V^{-1}]_{PQ} \tag{36}$$

The two-index two-electron density $\gamma^{\eta,y}_{PQ}$ is defined as

$$\gamma^{\eta,y}_{PQ} = \sum_{\alpha\beta}\Delta^{P,\eta,y}_{\alpha\beta}\sum_R(\alpha\beta|R)[V^{-1}]_{RQ} \tag{37}$$

3. IMPLEMENTATION

3.1. Calculation of Perturbed One-Electron Densities. The virtual−virtual and occupied−occupied blocks of the density $D^{F,\eta,y}$ contain contractions of the doubles Lagrangian multipliers and the response of the doubles amplitudes

$$D^{F,\eta,y}_{ij} = -\sum_a \bar{t}^y_{aj}t^y_{ai} - \sum_{abk}\bar{t}^{ab}_{jk}t^{y,ab}_{ik} \tag{38}$$

$$D^{F,\eta,y}_{ab} = \sum_i \bar{t}^y_{ai}t^y_{bi} + \sum_{cij}\bar{t}^{ac}_{ij}t^{y,bc}_{ij} \tag{39}$$

Since the derivatives of the doubles amplitudes depend on the unperturbed doubles amplitudes, the contraction with the Lagrangian multipliers contains three four-index quantities with different sets of indices. This cannot be evaluated efficiently without either storing or decomposing at least one of them. As described in more detail in ref 36, we use a numerical Laplace decomposition of the denominator in eq 5 as[41,42]

$$t^{ab}_{ij} = -\frac{\sum_Q \hat{B}^Q_{ai}\hat{B}^Q_{bj}}{\varepsilon_a - \varepsilon_i + \varepsilon_b - \varepsilon_j} \approx -\sum_Q \hat{B}^Q_{ai}\hat{B}^Q_{bj}\sum_\alpha^{N_\alpha}\omega_\alpha\, e^{-(\varepsilon_a-\varepsilon_i)\theta_\alpha}\, e^{-(\varepsilon_b-\varepsilon_j)\theta_\alpha} \tag{40}$$

with N_α sampling points θ_α and weights ω_α. Inserting eq 40 into eq 31 and forming intermediates $\hat{K}$ and $\bar{K}$ according to

$$\hat{K}^{Q,\alpha}_{ai} = \hat{B}^Q_{ai}\, e^{-(\varepsilon_a-\varepsilon_i)} \tag{41}$$

$$\bar{K}^{Q,\alpha.x}_{ai} = \sum_b \hat{K}^{Q,\alpha}_{bi}F_{ab}[\hat{f}^x] - \sum_j \hat{K}^{Q,\alpha}_{aj}F_{ji}[\hat{f}^x] \tag{42}$$

dx.doi.org/10.1021/ct400034t | J. Chem. Theory Comput. 2013, 9, 1469−1480

we obtain an expression which enables us to avoid storage of large intermediates also for this contribution to the one-electron density. As will be shown below, the numerical Laplace transformation introduces only negligible errors. The contribution to the one-electron densities can thus be evaluated as

$$D_{ab}^{\eta,(x)} = \sum_{i} \bar{t}_{ai} t_{bi}^{x} - \sum_{cij} \bar{t}_{ij}^{ac} \hat{P}_{ij}^{bc} \sum_{Q} \left(\sum_{\alpha} \hat{K}_{bi}^{Q,\alpha} \bar{K}_{cj}^{Q,\alpha,x} + (\hat{B}_{bi}^{Q}[\hat{J}^{x}] + \bar{B}_{bi}^{Q,x}) \hat{B}_{cj}^{Q} \right) (\varepsilon_b - \varepsilon_i + \varepsilon_c - \varepsilon_j)^{-1} \tag{43}$$

An alternative approach is to choose U_{pq}^{x} such that $F_{pq}[\hat{J}^{x}]$ is kept diagonal, which is possible if there are no near degeneracies in the occupied molecular orbitals. In this case, the expression for the one-electron density becomes

$$D_{ab}^{\eta,(x)} = \sum_{i} \bar{t}_{ai} t_{bi}^{x} - \sum_{cij} \bar{t}_{ij}^{ac} \hat{P}_{ij}^{bc} \left(\sum_{d} t_{ij}^{bd} F_{dc}[\hat{J}^{x}] - t_{ij}^{bc} \varepsilon_j^{x} + \sum_{Q} (\hat{B}_{bi}^{Q,(x)} + \bar{B}_{bi}^{Q}) \hat{B}_{cj}^{Q} \right) (\varepsilon_b - \varepsilon_i + \varepsilon_c - \varepsilon_j)^{-1} \tag{44}$$

where ε_p^{x} are the first derivatives of the orbital energies. In eq 44, unperturbed and perturbed doubles amplitudes have the same set of occupied orbital indices which enables the calculation of the one-electron density without storage of $\mathcal{N}^4$-scaling arrays or Laplace-transformation. The two approaches to calculate the perturbed one-electron densities have been discussed in more detail in ref 36.

3.2. Contractions of Three-Index Densities. The contributions to eqs 16 and 35 which contain the three-index densities $\Delta_{\alpha\beta}^{Q}$ and their perturbed analogs are as such not precomputed as complete arrays and stored on disc due to the large amount of memory the storage of these quantities would require. For 2-paracyclophane in the cc-pVTZ basis, an example that will be presented in section 4, 187 densities of this type would be needed (one resulting from the ground state, 93 of the type $\Delta^{Q,[x]}$, and 93 of the type $\Delta^{Q,\eta}$). Altogether this would require 1.3 TB of disc space. To avoid this, the densities are rewritten as intermediates where one AO index is replaced by an occupied MO index which for typical basis sets used for MP2 and CC2 calculations reduces the storage demands by about a factor of 4−16 (*vide infra*). Only for the contraction with the AO integrals is the three-index density in the AO basis constructed on-the-fly and immediately contracted with the integrals. The expressions for the unperturbed density $\Delta_{\alpha\beta}^{Q}$ are described in ref 33. $\Delta_{\alpha\beta}^{Q,[x]}$ is evaluated as

$$\Delta_{\alpha\beta}^{Q,[x]} = \sum_{j} (\Lambda_{\alpha j}^{p} \tilde{\Gamma}_{j\beta}^{Q,[x]} + \check{\Gamma}_{j\alpha}^{Q,[x]} \Lambda_{\beta j}^{h} + \check{\Lambda}_{\alpha j}^{p} \Gamma_{j\beta}^{*,Q,[x]}) \tag{45}$$

and $\Delta_{\alpha\beta}^{Q,\eta,[x]}$ as

$$\Delta_{\alpha\beta}^{Q,\eta,[x]} = \sum_{j} (\Lambda_{\alpha j}^{p} \tilde{\Gamma}_{j\beta}^{Q,\eta,[x]} + \check{\bar{\Gamma}}_{j\alpha}^{Q,\eta,[x]} \Lambda_{\beta j}^{h} + \check{\Gamma}_{j\alpha}^{Q,\eta} \bar{\Lambda}_{\beta j}^{h} + \check{\Lambda}_{\alpha j}^{p} \Gamma_{j\beta}^{*,Q,\eta,[x]}) \tag{46}$$

Explicit expressions for the intermediates Γ are given in the Supporting Information. Note that in the case of an MP2 calculation, only $\check{\Gamma}_{j\alpha}^{Q,[x]}$ in eq 45 and $\tilde{\Gamma}_{j\beta}^{Q,\eta,[x]}$ in eq 46 are nonzero. Thus, for the 2-paracyclophane example mentioned above, 75 GB of disc space are sufficient to store all Γ intermediates in an MP2 Hessian calculation. A CC2 calculation requires 300 GB of disc space, which is still a significant reduction compared to 1.3 TB.

3.3. Laplace Error. The sampling points θ_α for the numerical Laplace transformation described in section 3.1 are obtained by minimizing the mean squared error[41]

$$F^{\mathrm{Lap}}(\theta_\alpha, \omega_\alpha) = \int_{\varepsilon_{\min}}^{\varepsilon_{\max}} \left(\frac{1}{x} - \sum_{\alpha}^{N_\alpha} \omega_\alpha \mathrm{e}^{-x\theta_\alpha} \right)^2 \mathrm{d}x \tag{47}$$

where $\varepsilon_{\min}$ and $\varepsilon_{\max}$ are, respectively, twice the minimum and the maximum difference between any virtual and occupied orbital energy as described in ref 42.

To benchmark the error introduced by the numerical Laplace transformation, we performed a series of calculations on a set of aromatic hydrocarbons. For MP2, our main goal was to find a relation between F^{Lap} and the error in the calculated Hessian elements and frequencies. In this calculation, we varied F^{Lap} and investigated the deviation of the symmetry-allowed Hessian elements to a tightly converged result (F^{Lap} lower than 10^{-20}). We then evaluated the mean absolute error in the harmonic vibrational frequencies and in the Hessian elements relative to these reference results for various numbers of grid points. For MP2, calculations were done for thiophene, *p*-amino-nitrobenzene (ANB), hexafluorobenzene (C_6F_6), and naphthacene. These calculations were carried out in the cc-pVDZ orbital[46,47] and auxiliary basis set,[48,49] and the frequencies were not scaled.

The results for the frequencies are plotted in Figure 1, and a graphical overview of the errors for the Hessian elements is

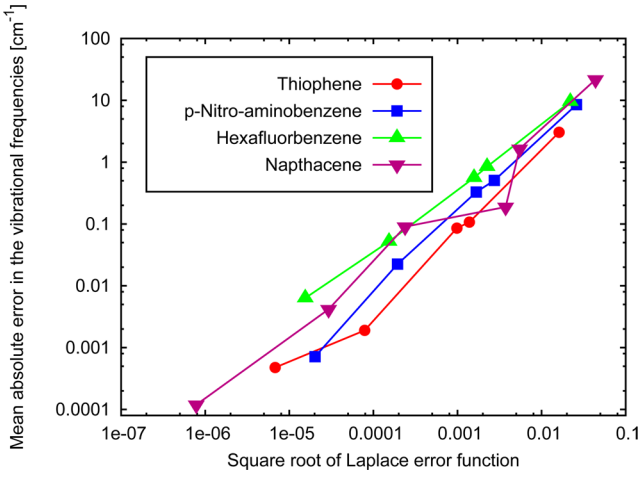

Figure 1. Mean absolute error in the vibrational frequencies for thiophene, ANB, C_6F_6, and naphthacene calculated with MP2.

given in the Supporting Information. The error in both the Hessian elements and the harmonic frequencies behave similarly and are over a wide range proportional to $(F^{\mathrm{Lap}})^{1/2}$ with a prefactor which varies only slightly between the four molecules, in particular for the Hessian elements. With a value of $(F^{\mathrm{Lap}})^{1/2} \leq 10^{-4}$, an average error of 10^{-7} au can be realized for the Hessian elements, which corresponds to the use of six sampling points for ANB, thiophene, and naphthacene, while for hexafluorobenzene eight sampling points are used. For the vibrational frequencies, an accuracy of ∼1 cm^{-1} is reached for

$(F^{\mathrm{Lap}})^{1/2} \leq 10^{-3}$ in all cases, which corresponds to the use of about three to four sampling points. However, if an accuracy of 0.01 cm^{-1} is seeked, $(F^{\mathrm{Lap}})^{1/2}$ should be 10^{-5} or less, which corresponds to about six sampling points. Since the calculation time for the one-particle densities $D^{F,\eta}$, which is the most time-consuming step in the whole calculation, depends linearly on the number of sampling points, this almost doubles the calculation time. The behavior of the Hessian elements is very similar to the one of the frequencies.

From the data plotted in Figure 1, we can estimate for the mean absolute error in the frequencies Δ^{MAD} an upper bound as

$$\Delta^{\mathrm{MAD}} \lessapprox 500\mathrm{cm}^{-1}\sqrt{F^{\mathrm{Lap}}} \tag{48}$$

For the CC2 method, we are interested in a relation between F^{Lap} and the threshold for the numerical solution of the linear equation system for the determination of the first derivatives of the cluster amplitudes T_{LRE}, which is defined as (see eq 26)

$$\|(\mathbf{A}^{\mathrm{eff}} - \omega\mathbf{1})t^x - x^{x,\mathrm{eff}}\| \leq T_{\mathrm{LRE}} \tag{49}$$

and is in the CC2 response calculation the main threshold that determines the numerical accuracy. Therefore, in a calculation series on thiophene, hexafluorobenzene, and ANB, both T_{LRE} and F^{Lap} were varied. Again, these calculations were done in the cc-pVDZ orbital and auxiliary basis sets, and the mean absolute deviations of the Hessian elements were evaluated. The results for thiophene are plotted for several values of T_{LRE} as a function of $(F^{\mathrm{Lap}})^{1/2}$ in Figure 2. The plots for hexafluorobenzene and p-amino-nitrobenzene look very similar and are given in the Supporting Information.

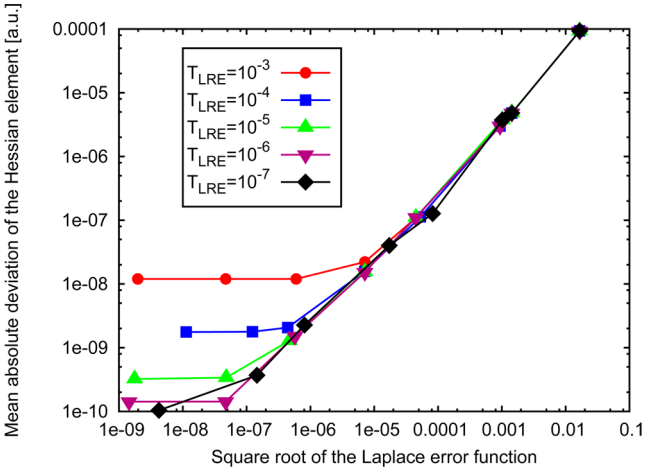

Figure 2. Mean absolute deviation of the CC2-Hessian elements in thiophen as a function of $(F^{\mathrm{Lap}})^{1/2}$.

We find that all curves are essentially linear in $(F^{\mathrm{Lap}})^{1/2}$ if this value is large compared to T_{LRE}, indicating that in this regime the deviation from the reference results is dominated by the Laplace error. If $(F^{\mathrm{Lap}})^{1/2}$ decreases to a certain level depending on T_{LRE}, we observe a flattening of the curve, which indicates that a regime is reached where the error is dominated by the residual error in the response equation, which is controlled by T_{LRE}. This enables us to formulate an upper bound for the mean absolute deviations in the Hessian elements $\Delta^{\mathrm{MAD}}_{\mathrm{Hess,CC2}}$:

$$\Delta^{\mathrm{MAD}}_{\mathrm{Hess,CC2}} \lessapprox 10^{-4}(T_{\mathrm{LRE}} + 100\sqrt{F^{\mathrm{Lap}}}) \tag{50}$$

A mean absolute error of 10^{-7} or lower in the Hessian elements can be obtained at a value of 10^{-5} for $(F^{\mathrm{Lap}})^{1/2}$, which corresponds to the use of six sampling points for thiophene and seven sampling points for hexafluorobenzene and ANB and a relatively loose convergence threshold for the first-order amplitude equations of $T_{\mathrm{LRE}} = 10^{-3}$.

4. APPLICATIONS

4.1. Fluoro-organic Compounds. Standard density functional approaches have known deficiencies in the description of the nonbonding dispersion interactions between the lone pairs of those atoms which are supposed to have a significant influence on the vibrational spectrum. Examples are trifluoromethyl groups where three fluorine atoms are crowded at one carbon center.

3,5-Bis(trifluoromethyl)pyrazole (BTFP) has been studied earlier both computationally and experimentally by Alkorta and co-workers.[50] The molecular structure is shown in Figure 3. We

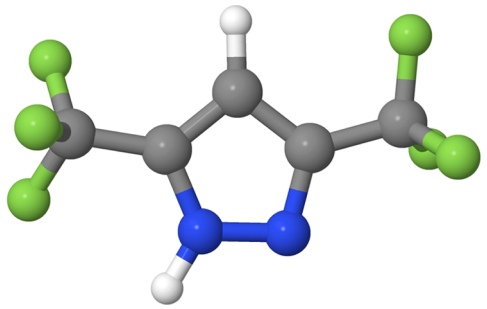

Figure 3. 3,5-Bis(trifluoromethyl)pyrazole (BTFP).

used for the current work the cc-pVTZ orbital[46] and auxiliary basis set[48] and MP2 as well as spin-component scaled MP2,[51] which is also available in our implementation. For comparison, we also computed the vibrational spectrum with B3LYP. All spectra were computed at a geometry optimized at the same level of theory. In the correlated wave function calculations, the 1s orbitals of C, O, N, and F were kept frozen. The DFT calculation took 3:25 h on one CPU core, while the MP2 calculation took 5:11 h using four CPU cores. All calculations were performed on Intel Xeon E5435 CPU cores with 2.33 GHz.

The vibrational frequencies from the B3LYP, MP2, and SCS-MP2 calculations have been scaled with the factors proposed by Merrick et al.[8] listed in Table 1 in order to account for anharmonicity and the error due to the method. For the SCS-MP2 calculations, we used the same scaling factors as for the MP2 calculations. The calculated vibrational frequencies and infrared intensities of BTFP are given in the Supporting Information. For a comparison with experimental data, theoretical spectra were generated from the calculated

Table 1. Scaling Factors for Vibrational Frequencies According to Ref 8

		scaling factor	
method	basis set	0−1000 cm^{-1}	above 1000 cm^{-1}
B3LYP	cc-pVDZ	1.0107	0.9717
B3LYP	cc-pVTZ	1.0066	0.9682
MP2	cc-pVDZ	0.9970	0.9538
MP2	cc-pVTZ	0.9956	0.9561

dx.doi.org/10.1021/ct400034t | J. Chem. Theory Comput. 2013, 9, 1469−1480

frequencies by superposition of Gaussians with heights corresponding to the computed intensities. The experimental spectrum was obtained similarly from frequency and intensity data from ref 50. A comparison of these spectra is shown in Figure 4.

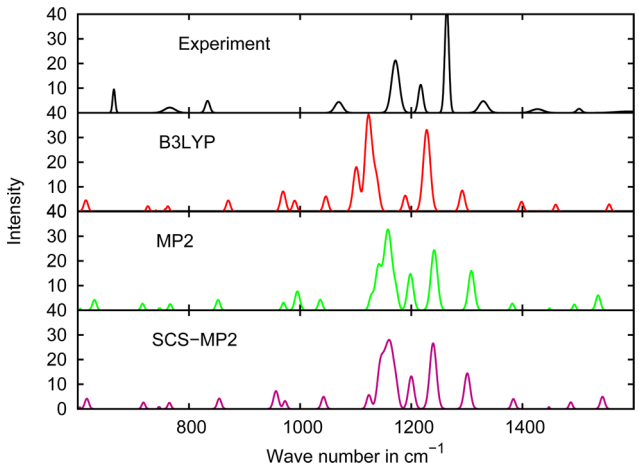

Figure 4. IR spectra of BTFP calculated from experimental data and from B3YLP, MP2, and SCS-MP2 calculations with the frequencies below 600 cm^{-1} and above 1600 cm^{-1} being cut off for clarity.

From Figure 4, we see that in the region above 1050 cm^{-1} the qualitative agreement between the results from MP2 and SCS-MP2 and the experimental frequencies is significantly better than with DFT/B3LYP. The corresponding normal modes describe C−F stretches. They are predicted between 1140 cm^{-1} and 1171 cm^{-1} by MP2 and between 1100 cm^{-1} and 1137 cm^{-1} by B3LYP. The experimental gas phase spectrum by Alkorta et al. shows an intensive band at 1171 cm^{-1}, which is about 10 cm^{-1} higher than the most intensive band in the MP2 spectrum.[50] For the two other intense bands above 1200 cm^{-1}, the frequencies from MP2 and SCS-MP2 are also in better agreement with experimental data than the B3LYP frequencies: the bands at 1227 cm^{-1} (B3LYP) and 1241 cm^{-1} (MP2), respectively, belong to a N−N stretch mode with contributions from a symmetric deformation mode of the trifluoromethyl groups. In this region, the experimental spectrum shows a band at 1264 cm^{-1}. An explanantion for the higher frequencies in MP2 is that this method takes into account the nonbonding dispersion interactions between the fluorine atoms. Comparing the MP2- and the SCS-MP2 spectra in Figure 4, we note that the theoretical spectra are very similar with most frequency shifts from MP2 to SCS-MP2 modifying the results slightly toward the experimental values.

The vibrational spectrum of perfluoro(isopropyl)-trifluoroactylperoxide has been studied in the gas phase by Minkwitz and Reinemann.[52] In the following, we will refer to this molecule as PTAP. A mapping of the potential energy surface revealed two minima which differ in the orientation of the perfluorinated isopropyl group. The MP2 geometries are shown in Figure 5; some additional results are summarized in Table 2.

Table 2. Geometry Data for Different Conformers of PTAP[a]

method	conformer (5)	OOCF [deg]	peroxo [deg]	relative energy [(kJ/mol)]	Boltzmann weights
B3LYP	a	−67.4	121.7	0.26	47%
B3LYP	b	68.9	149.1	0	53%
MP2	a	−68.9	106.4	0	65%
MP2	b	69.7	134.9	1.6	35%

[a]Here, the same abbreviations as in Figure 5 are used. The contribution of the structures has been calculated from a Boltzmann term at 298 K. All calculations have been performed in the cc-pVTZ basis.

In the B3LYP calculations, both conformers have nearly the same energy, while in MP2 their energies differ by about 1.6 kJ mol^{-1}, which leads at room temperature to Boltzmann weights of almost 2:1.

We computed spectra using the cc-pVTZ basis set and the B3LYP, MP2, and CC2 methods. The 1s orbitals of C, O, and F were kept frozen in the CC2 and MP2 calculations. The B3LYP calculation took 6:48 h on one single CPU core, while the MP2 calculation ran for 23:09 h on four CPU cores. All calculations were performed on Intel Xeon machines with 2.33 GHz. In Figure 6, the theoretical spectra are compared with a

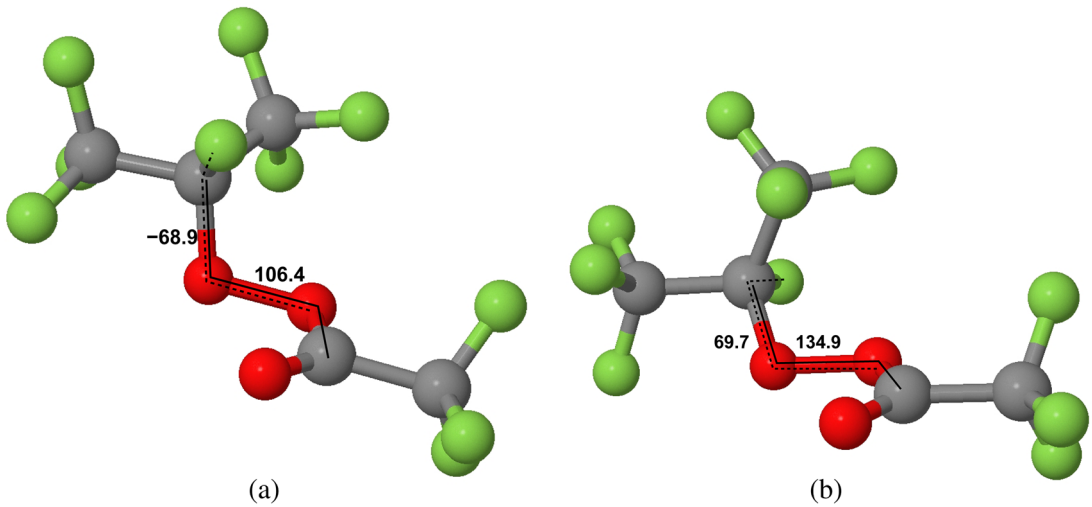

Figure 5. Conformers of perfluor(isopropyl)-trifluoracetylperoxid (PTAP). The angles are obtained from geometry optimizations using MP2. The OOCF dihedral is marked by the dotted line and the number on the left, while the dihedral on the peroxo group is marked with a solid line and the number on the right.

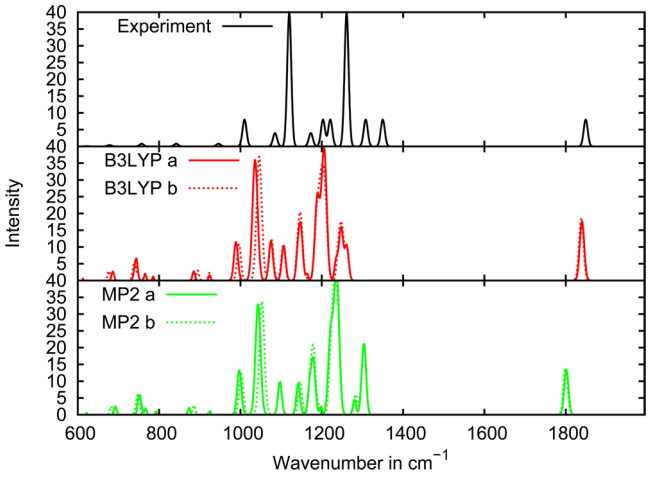

Figure 6. Theoretical IR spectrum of PTAB from calculations using MP2 and B3LYP with the cc-pVTZ basis set and a reconstruction of the experimental spectrum.

reconstruction of the experimental spectrum. This reconstruction was done since for the original spectrum only the frequencies and intensity classifications such as "strong" or "very weak" were available. These classifications were identified with appropriate numbers, and Gaussians with the corresponding height were plotted at the positions of the frequencies. Our calculated frequencies are listed in the Supporting Information. The computed vibrational frequencies discussed in the following are scaled with the factors given in Table 1.

From Figure 6, we note first that the deviations between the different conformers are very small. The largest deviation is found for the intensive band at 1050 cm^{-1}. Here, the frequencies differ by about 10 cm^{-1}. This band can be assigned to a CCO-deformation mode involving the peroxo group. Among the less intensive bands, two more normal modes could be identified which show deviations in the range of 10 cm^{-1}. All of these normal modes involve bendings in the peroxo group. Among the other normal modes, no deviations > 5 cm^{-1} could be found in the region above 600 cm^{-1}.

Comparing the MP2 and B3LYP results to experimental data, we find good agreement in the region between 0 and 1050 cm^{-1}, as can be seen from Figure 6. As an opposite in the spectral region between 1050 and 1400 cm^{-1}, we note significant red-shifts compared to the experimental results for both methods. The deviations are higher for B3LYP than for MP2. The beginning of a region with significant deviations between MP2 and B3LYP is marked by mode no. 37 (1096 cm^{-1} in MP2, 1075 cm^{-1} in B3LYP, for both conformers in both cases), which marks the beginning of the region with MP2 frequencies being significantly above the B3LYP ones. This band corresponds to the lowest C−F-stretching mode that could be found in the molecule.

Normal mode nos. 38−44 (1147−1240 cm^{-1} in MP2, 1105−1208 cm^{-1} in B3LYP) correspond to CF stretchings. The deviation between the MP2 and B3LYP values is 20−42 cm^{-1}. For normal mode nos. 45−47, the deviation is even higher. Mode no. 46 shows very similar intensities but a deviation of 53 cm^{-1} between the two methods. This region of the spectrum contains the CC stretching modes which are influenced by interactions with the trifluoromethyl groups. Both CF and CC stretchings have calculated frequencies significantly below the experimental ones with the MP2 results always closer to experimental data than B3LYP.

4.2. [2.2]-Paracyclophane. The [2.2]-paracyclophane molecule is of special interest because of the dispersion interactions between the two closely coupled benzene rings which have a significant influence on the vibrational frequencies. The vibrational spectrum of [2.2]-paracyclophane has been studied by infrared[53,54] and Raman spectroscopy[55] and via the fine structure of fluorescence spectra in the gas phase[56] and solid.[57] There have also been theoretical studies using density functional theory[58] and MP2.[59] The latter studies have been carried out using the basis sets 4-31G(d) and 6-31G. In the following, we present the results of the application of our Hessian implementation for CC2, MP2, and SCS-MP2 to [2.2]-paracyclophane using the correlation consistent cc-pVDZ and cc-pVTZ basis sets. In the correlated calculations, the 1s orbitals of the carbon atoms were kept frozen. As reported by Grimme, SCS-MP2 gives a structure for [2.2]-paracyclophane which is very close to the experimental one.[60] The complete results of our calculations are provided in the Supporting Information. A comparison of an experimental gas phase spectrum[61] with the current B3LYP and MP2 results is shown in Figure 7. If not stated otherwise, the computed harmonic vibrational frequencies have been scaled with the factors given in Table 1. Some characteristic frequencies are listed in Table 4.

The structure obtained with B3LYP differs significantly from those of the correlated wave function methods. While in the latter case the two aromatic rings of the molecule are twisted significantly, the structure from DFT shows only a very slight

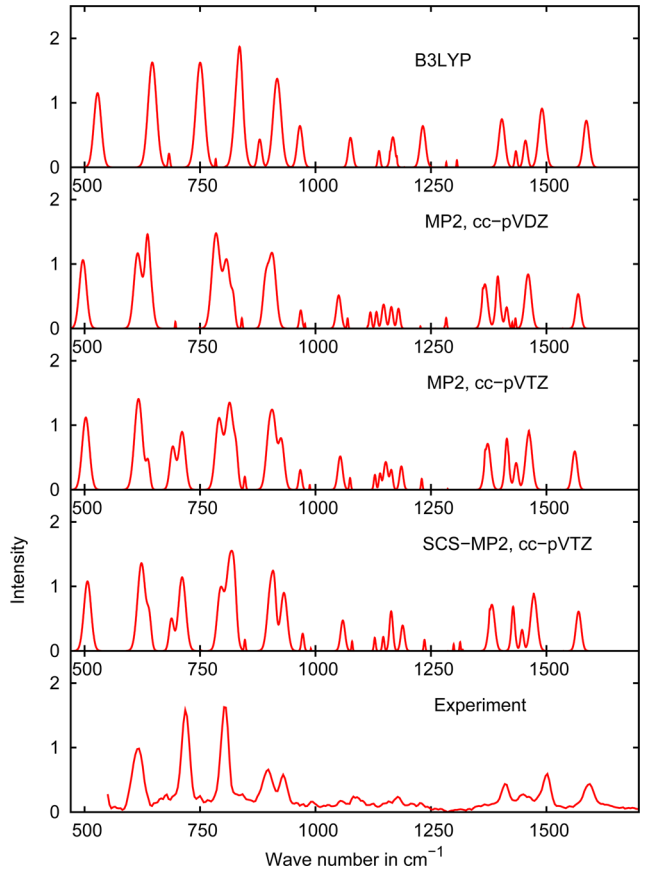

Figure 7. Comparison of the computed IR spectra (this study) of paracyclophane with the experimental data from ref 61.

dx.doi.org/10.1021/ct400034t | J. Chem. Theory Comput. 2013, 9, 1469−1480

twist. In Table 3, we have listed available theoretical and experimental results for the torsion angle δ (see Figure 8a).

Table 3. Torsion Angle δ (See Figure 8a) in the [2.2]-Paracyclophane Molecule from Different Methods and Experimental Data[a]

method	basis	δ [deg]	basis	δ [deg]	δ [deg]
B3LYP	cc-pVTZ	0.4	cc-pVDZ	1.45	3.9[58]
MP2	cc-pVTZ	18.6	cc-pVDZ	19.57	21.6[59]
SCS-MP2	cc-pVTZ	17.5	cc-pVDZ	18.22	
CC2	cc-pVTZ	19.6	cc-pVDZ	20.23	
experiment		16.2[59,62]			

[a]The values in the last column were calculated using the 4-31G(d) and 6-31G(d) basis sets, respectively.

Table 4. Frequencies (given in cm^{-1})[a]

MP2 cc-pVDZ	MP2	CC2	SCS-MP2	B3LYP	exptl.	remarks
242	241	241	239	238	240[56,57]	"breathing mode" of the macrocyclus
			strong basis set dependence			
647	708	697	707	742		"out-of-plane" deformation of aromatic rings
638	691	690	688	683		deformation of the macrocyclus
697	711	705	711	750	721	deformation of the macrocyclus

[a]All calculated frequencies were computed with the cc-pVTZ basis if not stated otherwise.

With the triple-ζ basis, B3LYP predicts a structure with nearly D_{2h} symmetry, while with the correlated wave function methods the structure is significantly twisted. Most transitions in the infrared spectrum of [2.2]-paracyclophane have very low intensities due to the high symmetry of the molecule. The most interesting mode in this respect is the so-called "breathing mode" of the macrocyclus, which is shown in Figure 8b. This mode is symmetry-forbidden in the IR spectrum. Nevertheless, Ron et al. could assign this mode to a vibration at 240 cm^{-1} by analyzing the vibrational fine structure of cooled [2.2]-paracyclophane single crystals.[56,57] This value is in excellent agreement with the current MP2 result of 241 cm^{-1}. The B3LYP result is with 234 cm^{-1} slightly lower. SCS-MP2 predicts this vibration at 238 cm^{-1} and (unscaled) CC2 at 239 cm^{-1}. The last result is in line with the general tendency of CC2 to give slightly smaller force constants than MP2.[33] In Table 4, we list the calculated frequencies.

Comparing the theoretical spectra with experimental data, we first note that in both the B3LYP and experimental spectra the bands are separated more clearly than in the spectra from MP2 and SCS-MP2. For the spectrum from B3LYP, this can be explained by the differences in structure between DFT and the correlated wave function based methods. On the other hand, the comparison of the experimental spectrum with computed harmonic frequencies is hindered by the only slightly hindered large amplitude twisting motion. At the MP2 level, the barrier is about 0.9 kJ mol^{-1} or 75 cm^{-1}. Nevertheless, Figure 7 shows that the spectra computed with MP2/cc-pVTZ and SCS-MP2/cc-pVTZ agree best with the experimental spectrum.

To study the basis set dependence of the MP2 results for the IR spectrum, we also did a calculation in the cc-pVDZ orbital and auxiliary basis set. The deviations between the frequencies are mostly below 10 cm^{-1}. In general, the intensities are more sensitive to the basis sets. Larger changes in the frequencies are observed between 500 and 1000 cm^{-1}, in particular for the bands around 700 cm^{-1}. In this region, MP2/cc-pVTZ predicts a bending mode of the macrocyclus at 708 cm^{-1}, which in the cc-pVDZ basis is found at 647 cm^{-1}. While in the cc-pVTZ basis two modes with b_4 symmetry at 691 cm^{-1} and 711 cm^{-1} have high intensities, the spectrum obtained with the cc-pVDZ basis has in this regime only one band with a high intensity and b_2 symmetry at 694 cm^{-1} and a rather weak band at 697 cm^{-1}. The corresponding normal modes are two deformations of the macrocylus. All other frequency shifts are less than 22 cm^{-1}, and in most cases, the cc-pVDZ results are red-shifted.

Since Grimme has emphasized the influence of spin-component scaling on the geometry of [2.2]-paracyclophane,[60] we also compare the spectrum obtained with SCS-MP2 with both the spectrum from MP2 and experimental data. We found that the results from MP2 and SCS-MP2 are very similar. Below 1600 cm^{-1}, we note a slight blue shift of the SCS-MP2 frequencies, while above 1600 cm^{-1} the SCS-MP2 frequencies are lower than the MP2 ones. In general, SCS-MP2 is found to reproduce experimental values better than MP2, which is in accordance with Grimme's findings.

4.3. Lanosterol. As a large scale application, we computed the IR spectrum of lanosterol. Its structure is shown in Figure 9. Lanosterol is part of the ISOL test set which was compiled by Huenerbein et al. as a benchmark for the calculation of reaction

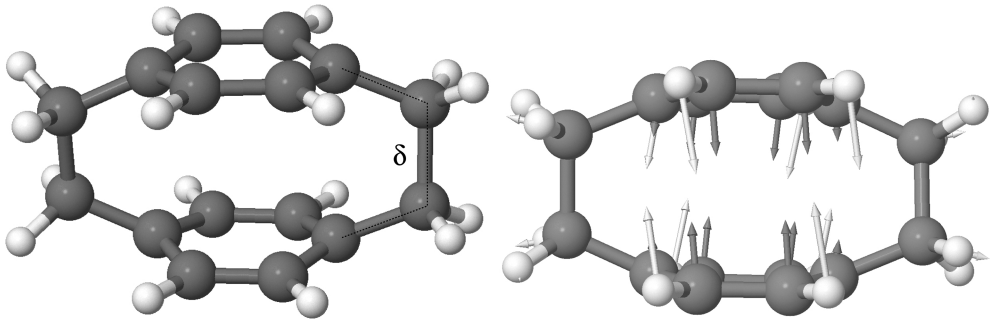

(a) Torsion angle δ (b) Breathing mode

Figure 8. Definition of the torsional angle δ in [2.2]-paracyclophane and visualization of the "breathing mode." All shown structures are from MP2 calculations.

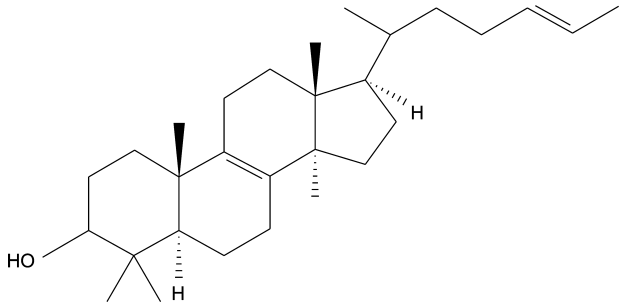

Figure 9. Structure of the lanosterol molecule.

energies with DFT.[63] This test set consists of 24 isomerization reactions of 48 molecules with up to 81 atoms. For the isomerization of lanosterol to an open-chain isomer, the DFT results deviated considerably from results obtained with wave function methods. Huenerbein et al. explained this by extensive intramolecular dispersion interactions within the compact lanosterol molecule which are neglected by DFT.

We optimized the structure with B3LYP, MP2, and SCS-MP2 in the cc-pVDZ basis and computed the vibrational spectra. The calculations have been done with frozen 1s orbitals at the carbon and oxygen atoms. The MO basis contained 684 functions, while the auxiliary basis consisted of 2436 functions. For the MP2 calculation, the first derivatives of the Fock matrix could be kept diagonal so that the numerical Laplace transformation could be replaced by the computationally cheaper canonical approach outlined in eq 44. On 12 Intel Xeon(R) X5675 CPU cores with 3.07 GHz, the calculation took 164 h. For SCS-MP2, the numerical Laplace transformation with five sampling points had to be used due to a near degeneracy in the occupied orbitals at the SCS-MP2 equilibrium geometry. This increased the wall time to 243 h on the same machine. Detailed tables with the frequencies and intensities are provided in the Supporting Information. The vibrational frequencies discussed in the following were scaled with the factors from Table 1. The computed spectra of lanosterol are shown in Figure 10 for the region between 0 cm^{-1} and 1750 cm^{-1}. An experimental spectrum which was measured in a KBr pellet for frequencies above 400 cm^{-1} is included for comparison.[64,65]

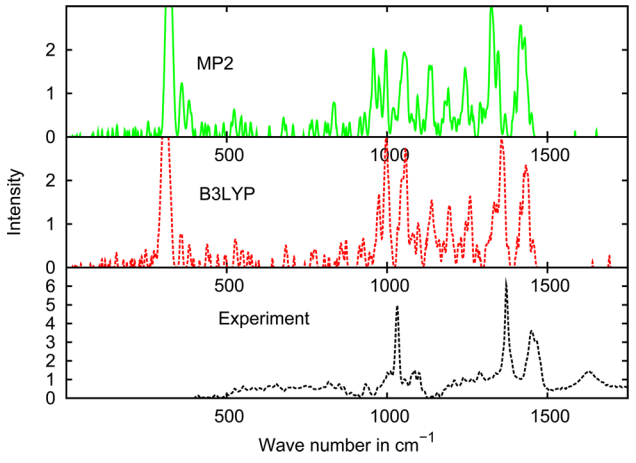

Figure 10. Theoretical and experimental IR spectrum for lanosterol between 0 cm^{-1} and 1750 cm^{-1}: region of skeletal and deformation vibrations.

The two very weak bands of the theoretical spectrum on the right-hand side of Figure 10 correspond to the CC-stretching modes of the two double bonds (MP2: 1586 cm^{-1}, 1658 cm^{-1}; SCS-MP2: 1597 cm^{-1}, 1660 cm^{-1}; B3LYP: 1641 cm^{-1}, 1693 cm^{-1}). Here, the strongest deviation between the MP2 and B3LYP methods was found with B3LYP overshooting MP2 by far. The experimental spectrum shows only a broad weak band at 1629 cm^{-1} which is in the region of the MP2 frequencies, while the B3LYP frequencies are considerably blue-shifted. Comparing the computed spectra with the experimental one, we find that the majority of the bands are reproduced at least qualitatively. Between 900 cm^{-1} and 1500 cm^{-1}, both MP2 and B3LYP give results below the experimental values with slightly larger devations for MP2. The spectra obtained with MP2 and SCS-MP2 show only relatively small differences. But in general the spin-component scaling leads to a slightly better agreement with the experimental frequencies.

5. CONCULSION AND OUTLOOK

An implementation of analytic second derivatives for MP2 and CC2 has been presented. It is to our knowledge for both MP2 and CC2 the first implementation of molecular Hessians which exploits the RI approximation for the computation of two-electron integrals and their derivatives. The storage of doubles amplitudes and their derivatives which would introduce $\mathcal{N}^4$-scaling memory or disc space demands is avoided by using a numerical Laplace transformation of orbital energy denominators. This approximation is shown to introduce only negligible errors in the final results.

Our implementation has been tested on two molecules that contain several trifluoromethyl groups as well as on [2.2]-paracyclophane and lanosterol as large-scale applications. The MP2 and SCS-MP2 results for the vibrational frequencies agree with the experimental results for the C−F stretch frequencies in general better than the B3LYP values. For the two hydrocarbon molecules also most vibrational modes which are strongly influenced by weak intramolecular dispersion interactions are more accurately described with the correlated wave function methods.

The new implementation extends the applicability of analytic Hessian calculations with MP2 and CC2 toward significantly larger molecules. The MP2 vibrational spectra of molecules with up to 80 atoms can even on standard Linux workstations be computed within less than two weeks. This also opens further perspectives for the computation of vibrational spectra with double hybrid density functionals, as the extension of the proposed techniques to such functionals is straightforward. It also paves the way to a variety of future applications. Analytic molecular Hessians are essential for a stable numerical calculation of higher-order derivatives, e.g., for anharmonic force fields. For an accurate treatment of intermolecular complexes, the calculation of vibrational frequencies with correlated wave function methods or density functionals that included orbital-dependent correlation contributions to account for dispersion interactions are desirable. An analytic evaluation of Hessians will also be helpful for excited states, where numerical differentiation techniques may easily fail due to root switching.

■ ASSOCIATED CONTENT

Supporting Information

Additional definitions and figures as well as calculated infrared spectrum data. This information is available free of charge via the Internet at http://pubs.acs.org.

■ AUTHOR INFORMATION

Corresponding Author

*E-mail: daniel.friese@ruhr-uni-bochum.de; christof.haettig@rub.de; joerg.kossmann@rub.de.

Notes

The authors declare no competing financial interest.

■ ACKNOWLEDGMENTS

The authors acknowledge support by the Deutsche Forschungsgemeinschaft (DFG) through grant HA 2588/5-1 and the collaborative research center SFB 558. D.H.F. is grateful to the Studienstiftung des Deutschen Volkes for a Ph.D. fellowship.

■ REFERENCES

(1) Deglmann, P.; Furche, F.; Ahlrichs, R. *Chem. Phys. Lett.* **2002**, *362*, 511−518.
(2) Dirac, P. A. M. *Proc. R. Soc. London, Ser. A* **1929**, *123*, 714−733.
(3) Slater, J. C. *Phys. Rev.* **1951**, *81*, 385−390.
(4) Vosko, S. H.; Wilk, L.; Nusair, M. *Can. J. Phys.* **1980**, *58*, 1200−1211.
(5) Becke, A. D. *Phys. Rev. A* **1988**, *38*, 3098−3100.
(6) Lee, C.; Yang, W.; Parr, R. G. *Phys. Rev. B* **1988**, *37*, 785−789.
(7) Scott, A. P.; Radom, L. *J. Phys. Chem.* **1996**, *100*, 16502−16513.
(8) Merrick, J. P.; Moran, D.; Radom, L. *J. Phys. Chem. A* **2007**, *111*, 11683−11700.
(9) Halls, M. D.; Schlegel, H. B. *J. Chem. Phys.* **1998**, *109*, 10587−10593.
(10) Johnson, E. R.; DiLabio, G. A. *Chem. Phys. Lett.* **2006**, *419*, 333.
(11) Grimme, S. *J. Chem. Phys.* **2006**, *124*, 034108.
(12) Eshuis, H.; Yarkony, J.; Furche, F. *J. Chem. Phys.* **2010**, *132*, 234114.
(13) Pulay, P. *Mol. Phys.* **1969**, *17*, 197−204.
(14) Bishop, D. M.; Randič, M. *J. Chem. Phys.* **1966**, *44*, 2480−2487.
(15) Stanton, J. F.; Gauss, J. *Int. Rev. Phys. Chem.* **2000**, *19*, 61−95.
(16) Handy, N.; Amos, R.; Gaw, J.; Rice, J.; Simandiras, E. *Chem. Phys. Lett.* **1985**, *120*, 151−158.
(17) Harrison, R. J.; Fitzgerald, G. B.; Laidig, W. D.; Bartlett, R. J. *Chem. Phys. Lett.* **1986**, *124*, 291−294.
(18) Jørgensen, P.; Helgaker, T. *J. Chem. Phys.* **1988**, *89*, 1560−1570.
(19) Helgaker, T.; Jørgensen, P.; Handy, N. C. *Theor. Chem. Acc.* **1989**, *76*, 227−245.
(20) Koch, H.; Jensen, H. J. A.; Jørgensen, P.; Helgaker, T.; Scuseria, G. E.; Schaefer, H. F., III *J. Chem. Phys.* **1990**, *92*, 4924−4940.
(21) Kállay, M.; Gauss, J. *J. Chem. Phys.* **2004**, *120*, 6841−6848.
(22) Gauss, J.; Stanton, J. F. *Chem. Phys. Lett.* **1997**, *276*, 70−77.
(23) Gauss, J.; Stanton, J. F. *Phys. Chem. Chem. Phys.* **2000**, *2*, 2047−2060.
(24) Christiansen, O.; Koch, H.; Jørgensen, P. *Chem. Phys. Lett.* **1995**, *243*, 409−418.
(25) Beebe, N. H. F.; Linderberg, J. *Int. J. Quantum Chem.* **1977**, *12*, 683−705.
(26) Whitten, J. L. *J. Chem. Phys.* **1973**, *58*, 4496−4501.
(27) Dunlap, B. I.; Connolly, J. W. D.; Sabin, J. R. *J. Chem. Phys.* **1979**, *71*, 3396−3402.
(28) Feyereisen, M.; Fitzgerald, G.; Komornicki, A. *Chem. Phys. Lett.* **1993**, *208*, 359−363.
(29) Vahtras, O.; Almlöf, J.; Feyereisen, M. *Chem. Phys. Lett.* **1993**, *213*, 514−518.
(30) Hättig, C.; Weigend, F. *J. Chem. Phys.* **2000**, *113*, 5154−5161.
(31) Hättig, C.; Köhn, A. *J. Chem. Phys.* **2002**, *117*, 6939−6951.
(32) Weigend, F.; Häser, M. *Theor. Chem. Acc.* **1997**, *97*, 331−340.
(33) Hättig, C. *J. Chem. Phys.* **2002**, *118*, 7751−7761.
(34) Köhn, A.; Hättig, C. *J. Chem. Phys.* **2003**, *119*, 5021−5036.
(35) Pedersen, T.; Sánchez de Meras, A. M. J. S.; Koch, H. *J. Chem. Phys.* **2004**, *120*, 8887−8897.
(36) Friese, D. H.; Winter, N. O. C.; Balzerowski, P.; Schwan, R.; Hättig, C. *J. Chem. Phys.* **2012**, *136*, 174106.
(37) Friese, D. H.; Hättig, C.; Ruud, K. *Phys. Chem. Chem. Phys.* **2012**, *14*, 1175−1184.
(38) Helgaker, T.; Jørgensen, P. *Theor. Chem. Acc.* **1989**, *75*, 111.
(39) Christiansen, O.; Jørgensen, P.; Hättig, C. *Int. J. Quantum Chem.* **1998**, *68*, 1−52.
(40) Helgaker, T.; Jørgensen, P.; Olsen, J. *Molecular Electronic Structure Theory*; J. Wiley and Sons: New York, 2000; p 13.
(41) Häser, M.; Almlöf, J. *J. Chem. Phys.* **1992**, *96*, 489−494.
(42) Winter, N. O. C.; Hättig, C. *J. Chem. Phys.* **2011**, *134*, 184101.
(43) Helgaker, T.; Jørgensen, P. *Adv. Quantum Chem.* **1988**, *19*, 183−244.
(44) Simons, J.; Jørgensen, P.; Helgaker, T. *Chem. Phys.* **1984**, *86*, 413−432.
(45) Hättig, C.; Christiansen, O.; Jørgensen, P. *J. Chem. Phys.* **1998**, *75*, 8331−8354.
(46) Dunning, T. H. *J. Chem. Phys.* **1989**, *90*, 1007−1023.
(47) Woon, D. E.; Dunning, T. H. *J. Chem. Phys.* **1993**, *98*, 1358−1371.
(48) Weigend, F.; Köhn, A.; Hättig, C. *J. Chem. Phys.* **2002**, *116*, 3175−3183.
(49) Hättig, C. *Phys. Chem. Chem. Phys.* **2005**, *7*, 59−66.
(50) Alkorta, I.; Elguero, J.; Donnadieu, B.; Etienne, M.; Jaffart, J.; Schagen, D.; Limbach, H.-H. *New J. Chem.* **1999**, *23*, 1231−1237.
(51) Grimme, S. *J. Chem. Phys.* **2003**, *118*, 9095−9102.
(52) Minkwitz, R.; Reinemann, S. *Z. Anorg. Allg. Chem.* **1998**, *624*, 1695−1698.
(53) Cram, D. J.; Steinberg, H. *J. Am. Chem. Soc.* **1951**, *73*, 5691−5704.
(54) Schettino, V.; Marzocchi, M.; Sbrana, G. *J. Mol. Struct.* **1968**, *2*, 39−45.
(55) Scudder, P. H.; Boekelheide, V.; Cornutt, D.; Hopf, H. *Spectrochim. Acta, Part A* **1981**, *37*, 425−435.
(56) Ron, A.; Noble, M.; Lee, E. K. *Chem. Phys.* **1984**, *83*, 215−219.
(57) Ron, A.; Schnepp, O. *J. Chem. Phys.* **1962**, *37*, 2540−2546.
(58) Walden, S. E.; Glatzhofer, D. T. *J. Phys. Chem. A* **1997**, *101*, 8233−8241.
(59) Henseler, D.; Hohlneicher, G. *J. Phys. Chem. A* **1998**, *102*, 10828−10833.
(60) Grimme, S. *Chem.—Eur. J.* **2004**, *10*, 3423−3429.
(61) Infrared Spectra. In *NIST Chemistry WebBook, NIST Standard Reference Database Number 69*; Linstrom, P. J., Mallard, W. G., Eds.; National Institute of Standards and Technology: Gaithersburg, MD. http://webbook.nist.gov (retrieved March 5, 2012).
(62) Hope, H.; Bernstein, J.; Trueblood, K. *Acta Crystallogr., Sect. B: Struct. Crystallogr. Cryst. Chem.* **1972**, *28*, 1733−1743.
(63) Huenerbein, R.; Schirmer, B.; Moellmann, J.; Grimme, S. *Phys. Chem. Chem. Phys.* **2010**, *12*, 6940−6948.
(64) Manea, M.; Chiosa, V.; Stănculescu, I.; Mandravel, C. *Rev. Roum. Chim.* **2009**, *54*, 399−403.
(65) Ioana Stănculescu (University of Bukarest), private communication.